Early-stage rifting of the northern Tyrrhenian Sea Basin: Results from a combined wide-angle and multichannel seismic study

S. Moeller and I. Grevemeyer
GEOMAR Helmholtz Centre for Ocean Research Kiel, Kiel DE-24148, Germany (smoeller@geomar.de)

C. R. Ranero
Barcelona Center for Subsurface Imaging, ICM, ICREA at CSIC, Barcelona, Spain

C. Berndt and D. Klaeschen
GEOMAR Helmholtz Centre for Ocean Research Kiel, Kiel DE-24148, Germany

V. Sallares
Barcelona Center for Subsurface Imaging, ICM, CSIC, Barcelona, Spain (smoeller@geomar.de)

N. Zitellini
Istituto Scienze Marine ISMAR-CNR, Bologna, Italy

R. de Franco
Istituto per la Dinamica dei Processi Ambientali, CNR, Milan, Italy

[1] Extension of the continental lithosphere leads to the formation of rift basins and ultimately may create passive continental margins. The mechanisms that operate during the early stage of crustal extension are still intensely debated. We present the results from coincident multichannel seismic and wide-angle seismic profiles that transect across the northern Tyrrhenian Sea Basin. The profiles cross the Corsica Basin (France) to the Latium Margin (Italy) where the early-rift stage of the basin is well preserved. We found two domains, each with a distinct tectonic style, heat flow and crustal thickness. One domain is the Corsica Basin in the west that formed before the main rift phase of the northern Tyrrhenian Sea opening (∼8–4 Ma). The second domain is rifted continental crust characterized by tilted blocks and half-graben structures in the central region and at the Latium Margin. These two domains are separated by a deep (∼10 km) sedimentary complex of the eastern portion of the Corsica Basin. Travel-time tomography of wide-angle seismic data reveals the crustal architecture and a subhorizontal 15–17 ± 1 km deep Moho discontinuity under the basin. To estimate the amount of horizontal extension we have identified the pre-, syn-, and post-tectonic sedimentary units and calculated the relative displacement of faults. We found that major faults initiated at angles of $45°$–$50°$ and that the rifted domain is horizontally stretched by a factor of $\beta \sim 1.3$ (∼8–10 mm/a). The crust has been thinned from ∼24 to ∼17 km indicating a similar amount of extension (∼30%). The transect represents one of the best imaged early rifts and implies that the formation of crustal-scale detachments, or long-lived low-angle normal faults, is not a general feature that controls the rift initiation of continental crust. Other young rift basins, like the Gulf of Corinth, the Suez Rift or Lake Baikal, display features resembling the northern Tyrrhenian Basin, suggesting that half-graben formations and distributed homogeneous crustal thinning are a common feature during rift initiation.

Components: 10,937 words, 12 figures, 1 table.

1. Introduction

[2] The formation of rift basins and rifted margins by normal faulting and crustal thinning has many open questions. To contribute to the understanding of basin evolution, investigations of early-stage continental rift settings are important. Numerous studies have shown that the amount of fault displacement imaged on seismic cross sections cannot easily explain the vertical crustal thinning estimated from wide-angle seismic studies. This phenomenon is known as the extension discrepancy [*White*, 1990; *Walsh et al.*, 1991; *Reston*, 2007]. Another observation is that rifts seem to be asymmetric in extensional style. Symmetry is mostly absent, for instance at the young Gulf of Corinth [*Bell et al.*, 2008], the North Sea rift [*Lister et al.*, 1991], or at the conjugate margins of Newfoundland and Iberia [*Shillington et al.*, 2006]. It has been proposed that rifts become asymmetric by the role of low-angle normal faulting in the early-stage [*Bosworth*, 1985], similar to the crustal-scale or lithospheric-scale simple-shear model [e.g., *Wernicke*, 1985]. This model has been very popular to explain the structure of numerous conjugate rifted margins in an upper and a lower plate margin corresponding to the large-scale hanging wall and footwall blocks of the detachment. Slip on low-angle normal faults ($<30°$) or large detachments would generate a large amount of horizontal extension and might explain the extension discrepancy. However, the existence of such detachments is a matter of debate because these types of faults have not been observed in young rift settings with an initially normal crustal thickness. *Allemand and Brun* [1991] showed that the initial fault angle can be controlled by the thickness of the brittle layer and hence can be less than 60°. *Buck* [1993] suggested that low-angle faults initiate at steeper angles and subsequently rotate to shallower angles. Alternative explanations argue that extension is not well estimated because of the limited resolution of seismic data and hence smaller faults or a previous generation of faults contributing to the total amount of extension is unrecognized [*Reston*, 2007; *Marett and Allmendinger*, 1992; *Walsh et al.* 1991]. An alternative to these models is that much of the extension is not caused by large arrays of faults working simultaneously, but as extension progresses, strain localizes into a relatively narrow rift center via sequential faulting [*Ranero and Pérez-Gussinye*, 2010]. This model proposes that individual successive faults cut crust that had been previously extended by earlier individual faults explaining the structure observed in West Iberia and New-foundland conjugate margins. The model explains both the apparent horizontal extension and the formation of asymmetric conjugate margins by simple Andersonian faulting at 65°–55° and rotating to 45°–30° as observed in seismic images. Sequential fault activity has also been observed in some young rift settings, for example the Suez Rift [*Gawthorpe et al.*, 2003].

[3] In this study, we have prestack depth migrated and interpreted a 190 km long multichannel seismic reflection line (MCS) and modeled a coincident 240 km long WAS profile across the northern Tyrrhenian Sea Basin to investigate the relationship between faulting, crustal thinning and basin formation in an early stage of continental extension. From the MCS images we determined the geometry of syn- and post-tectonic sediment and infer the evolution of rift structures.

2. Tectonic Framework and Bathymetric Features

[4] The Tyrrhenian Sea is the youngest extensional basin in the Western Mediterranean Sea [*Kastens et al.* 1988] bounded by Corsica and

Sardinia in the west, the Italian peninsula to the east and north and by Sicily to the south. Subduction of the Tethys Mesozoic oceanic lithosphere underneath the European plate commenced during the late Cretaceous [*Faccenna et al.*, 2001; *Jolivet et al.*, 1999] and triggered the episodic opening of several back-arc basins in the Western Mediterranean Sea due to the rollback and subsequent bending of the trench axis [*Faccenna et al.*, 2001]. The formation of extensional basins began along southern France and Iberia with the separation of the Balearic block and Sardinia and Corsica from continental Europe coupled with the opening of the Gulf of Lion and the Valencia Trough in the Oligocene ∼30 Ma ago [*Rosenbaum et al.*, 2002; *Cherchi and Montadert*, 1982]. Post-Oligocene (21–16 Ma) [*Faccenna et al.*, 2001] rifting in the Gulf of Lion and in the Ligurian Sea continued and the Sardinia-Corsica block of European continental crust underwent a counter-clockwise rotation of 30°, subsequently colliding with the Adriatic foreland. From the Langhian to Tortonian, continental sediments started folding and thrusting and led to the formation of the N-S striking Apennine orogenic belt along the Italian peninsula. Moreover, volcanic rocks on Sardinia are believed to be a remnant volcanic arc of the subduction process east of Sardinia [*Cherchi and Montadert*, 1982]. The eastward migration of the subduction zone led to the opening of the Tyrrhenian back-arc basin [*Malinverno and Ryan*, 1986; *Rosenbaum et al.*, 2002]. Rifting of the northern Tyrrhenian basin segment started during upper Tortonian age (∼8–9 Ma) and ceased in Early-Pliocene (∼5 Ma) [*Sartori*, 1990; *Rosenbaum et al.*, 2002]. This is seen in the Tyrrhenian basin by the widespread presence of two major unconformities that mark the start and the end of rifting [*Trincardi and Zitellini*, 1987].

[5] To the southeast, rifting proceeded toward the Calabrian arc (Figure 1a) with an increased gravity anomaly (Figure 1b). Here a narrow but well-defined Wadati-Benioff seismic zone and volcanic edifices in the Aeolian region indicate the existence of a subducted slab [*Faccenna et al.*, 2001; *Malinverno and Ryan*, 1986].

[6] The northern portion of the Tyrrhenian basin between Corsica, the Latium Margin and south of Elba Island is the main focus of this study (Figure 1). Based on the seafloor relief, the region is divided into two distinct areas: An area with relatively smooth topography that contains the Tus-

cany Archipelago and the flat Corsica Basin west of the islands and a second area to the south and east of the Corsica Basin that contains parallel N-S striking horst and graben structures across the center of the Tyrrhenian basin into the Latium Margin. The seafloor in the Corsica Basin is ∼900 m deep whereas the bathymetry in the east ranges from 360 m on the ridges to 1700 m in the sediment filled grabens. The Corsica Basin is bounded to the east by the sedimentary Pianosa Ridge (A1 in Figure 1). The island of Corsica consists of two parts: the Alpine part in the northeast and the Hercynian part in the southwest. These two parts are separated by the Solenzara fault that bounds the Corsica Basin to the south (Figure 1). The Pianosa Ridge is associated with prominent magnetic anomalies probably related to magmatic intrusions [*Mauffret et al.*, 1999], although the presence of an ophiolitic body may be another potential explanation (Figure 1). More than 200 heat flow measurements have been carried out in the Tyrrhenian Sea during the last decades [*Della Vedova et al.*, 1984]. The main feature in the northern Tyrrhenian Sea is a regional trend from low heat flux values at the margin of Sardinia and Corsica (50 mW/m^2), which is typical for old and cold continental crust [*Della Vedova et al.*, 1984], to higher heat flow values of 100–150 mW/m^2 toward the margin of the Italian peninsula [*Wang et al.*, 1989].

3. Seismic Data: Acquisition, Processing, and Analysis

3.1. Acquisition

[7] The new MCS and WAS data were acquired in the framework of the MEDOC project (El **MED**iterráneo **OC**cidental) during a two-ship experiment in April and May 2010. 22 GEOMAR ocean-bottom-hydrophones (OBH) were deployed from the Italian vessel RV Urania for the WAS experiment. The station spacing was 7–8 km. The Spanish vessel B/O *Sarmiento de Gamboa* provided additional ocean-bottom-seismometers (OBS) and fired shots every 90 s using an array consisting of two subarrays of 12 G.Gun II airguns with a total volume of 4600 in^3. In addition to the OBH stations, the profile was extended by using three land stations on Corsica (Figure 1c). A coincident marine MCS line was acquired using a 3450 m, 276-channel streamer with a group interval of 12.5 m. The source was a 3040 in^3 G.Gun II array. The shot interval was 50 m, resulting in a common-mid-point (CMP) fold of 35.
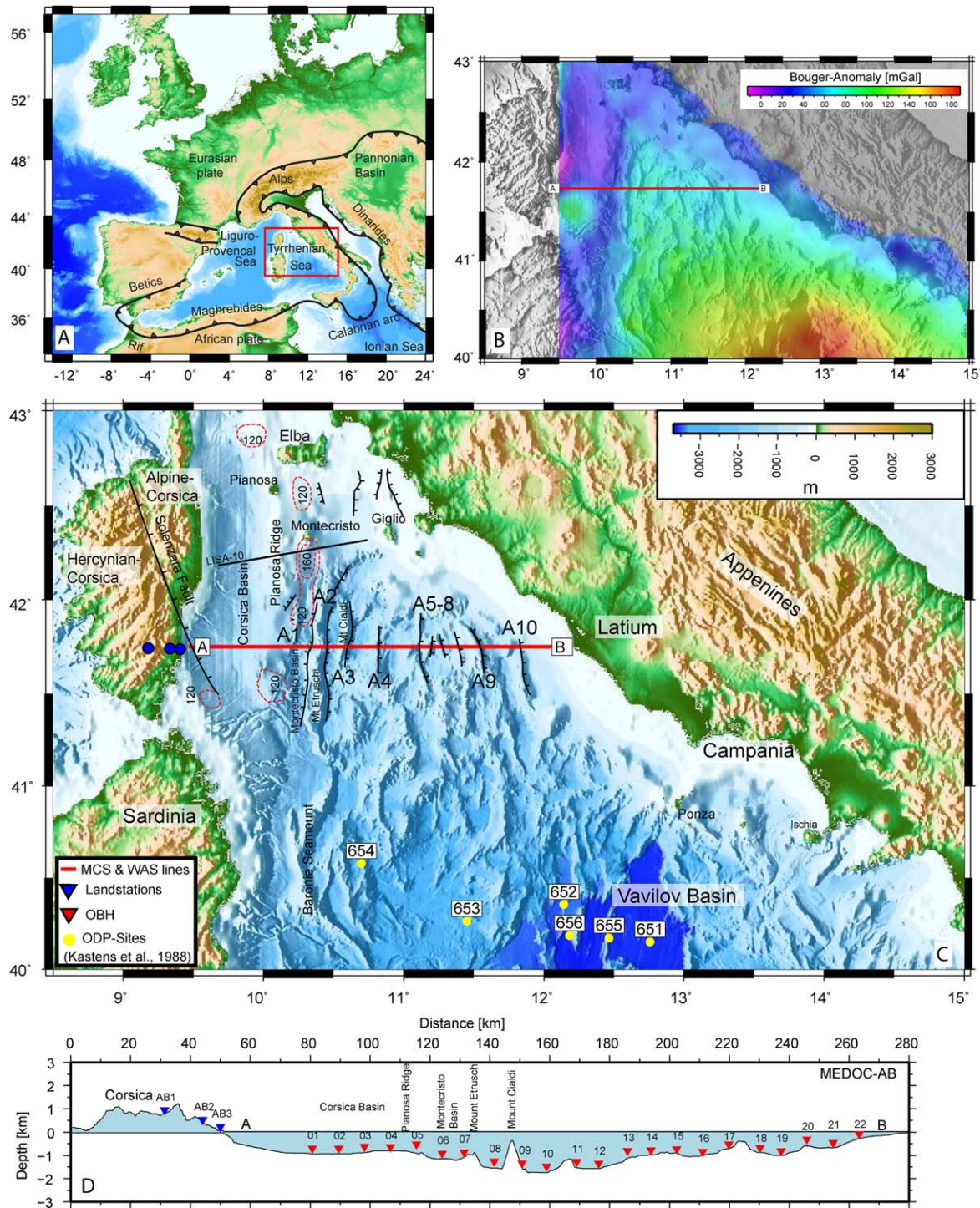
Figure 1. (a) The recent plate configuration of the Western Mediterranean region and central Europe. Plate boundaries after Schellart, 2010. The red box in the Tyrrhenian Sea defines the working area. (b) The map shows the Bouger-Anomaly in the northern and central region of the Tyrrhenian Sea which is increasing toward the SE. (c) The bathymetric map of the northern and central part of the Tyrrhenian Sea [Medimap]. The seismic transect (red line) crosses the main bathymetric rift features that are N-S orientated (Figures 3 and 7). The ridges (blocks) are labeled from A1 to A10. Orientations of major normal faults along the seismic transect come from this study. Other fault orientations after *Mauffret et al.* [1999]. The black line (LISA-10) marks the location of a previous refraction experiment after *Contrucci* et al. [2005]. Red dotted areas mark locations of high magnetic anomalies larger 120 nT (reduced to pole). Magnetic and gravity data is a courtesy of Getech UK. (d) The cross section shows the bathymetric features along the MEDOC-AB transect and the positions of the land and OBH stations. *Medimap* [2008], Morpho-bathymetry of the Mediterranean Sea. The plate boundaries in (A) and some fault-structures in (C) are after *Schellart* [2010] and *Mauffret* [1999]. Permissions for showing the gravity and magnetic data are given by Getech, UK.

3.2. Processing and Data Analysis

3.2.1. Refraction and Wide-Angle Reflection Seismic Data

[8] The WAS data recorded by the ocean-bottom-instruments were sampled at 4 and 5 ms in a continuous trace. Before and after recovery data loggers were synchronized with the Global Positioning System time signal to correct for internal clock drift. The data were cut into single receiver traces using the shot times and converted into SEG-Y format. The assumed position on the seafloor was corrected using the arrival times of the direct wave. To enhance the S/N ratio, a statistical deconvolution and a time- and offset-variant Butterworth filter were applied to the data. The deconvolution suppressed the reverberations of the airgun signal using a prediction lag of 0.23 s and an operator length of 1 s. The Butterworth filter moves within four windows toward lower frequencies as time and offset increase. For the near offset traces the bandpass ranged from 4 to 35 Hz and at far offsets from 2.5 to 14 Hz.

[9] Nearly all stations recorded data of good quality, except for OBH02 and OBH11 which failed to record any useful data. Record sections from OBH stations 03, 09, and 19 are presented in Figure 2. A sufficient S/N ratio allowed identification of first arrival crustal phases (Pg) between offsets of 30 and 120 km. First arrival branches in the near offset, that is, offsets less than ~30 km, show Pg phases with rapidly increasing velocities corresponding to a high velocity gradient in the upper part of the crust. First arrivals with an offset larger than ~30 km show that the velocity gradient at depth is smaller than in the upper part of the crust. A prominent secondary arrival between 40 and 80 km offset is interpreted as the wide-angle PmP reflection. The beginning of these high amplitude arrivals at 40 km offset is roughly the critical distance for reflections in the final tomographic model. Wide-angle PmP reflections are clearly observed on almost all OBH seismic records.

[10] Arrivals of refracted phases traveling through the upper mantle (Pn) at larger offsets cannot be identified. A late reflected arrival was recorded by stations OBH06 to OBH10 between 6–8 s and 60–80 km offset (see PimP at OBH09 in Figure 2). These arrivals were first interpreted as PmP reflections, but during modeling it was clear that they do not fit well to reflections from the crust-mantle boundary. Rather, they appear to come from a deep and steep intra-mantle reflector.

[11] Stations OBH01 to OBH05 are located in the western part of the profile at the Corsica Basin. Pg phases traveling through the basin are relatively slow and indicate the presence of a thick sediment pile. Here first arrivals can be observed up to offsets of 20–30 km. The seismogram of OBH05 (Figure 2) is an example of a station at the Corsica Basin. It shows that the velocities in the near offset range to the east are slower than to the west. Seismic arrivals at the stations east of the Corsica Basin differ from those located at the basin. They recorded faster Pg-phases and PmP-reflections over offset ranges up to 60 km. The influence of the lower velocities in the Corsica Basin at OBH09 is observed at ~40 km offset to the west where the first arrival slope is steeper. The land stations on Corsica recorded arrivals just over a short offset range (40–60 km) and can only contribute to determining the sediment velocity structure in the Corsica Basin. The pick uncertainties of the arrival times increase from 50 ms at near offsets to 100 ms at far offsets. These uncertainties also include phase changes and time shifts related to filtering and predictive deconvolution.

[12] After phase identification and picking we used the forward modeling code Rayinvr [Zelt and Smith, 1992] to build a reference "best fit" p wave velocity model that was subsequently refined by travel-time tomography. For this purpose we used the code tomo2-D [Korenaga et al. 2000] that jointly inverts for travel times of both refracted and reflected seismic phases. The seafloor and topography of Corsica was gridded at a spacing of 750 m. The velocity field was implemented as a sheared mesh grid with cells hanging below the seafloor topography. We chose a cell size of 200 m in the horizontal and 100 m in the vertical direction increasing to 500 m at ~30 km depth. To invert for PmP arrivals, the Moho is constrained as a floating reflector. The well determined geometry and velocities of the sedimentary sub-basins along the profile were adopted from the final depth-migrated MCS section and kept fixed during the forward modeling.

[13] Our subsequent inversion strategy followed a downward stripping approach by first inverting for the upper crustal arrivals and then successively for all deeper crustal arrivals. The effect of different smoothing and damping parameters as well as the interaction with the horizontal and vertical correlation lengths were tested for a broad set of parameters. The horizontal correlation lengths ranged from 1 km at the top of the model to 5 km at the
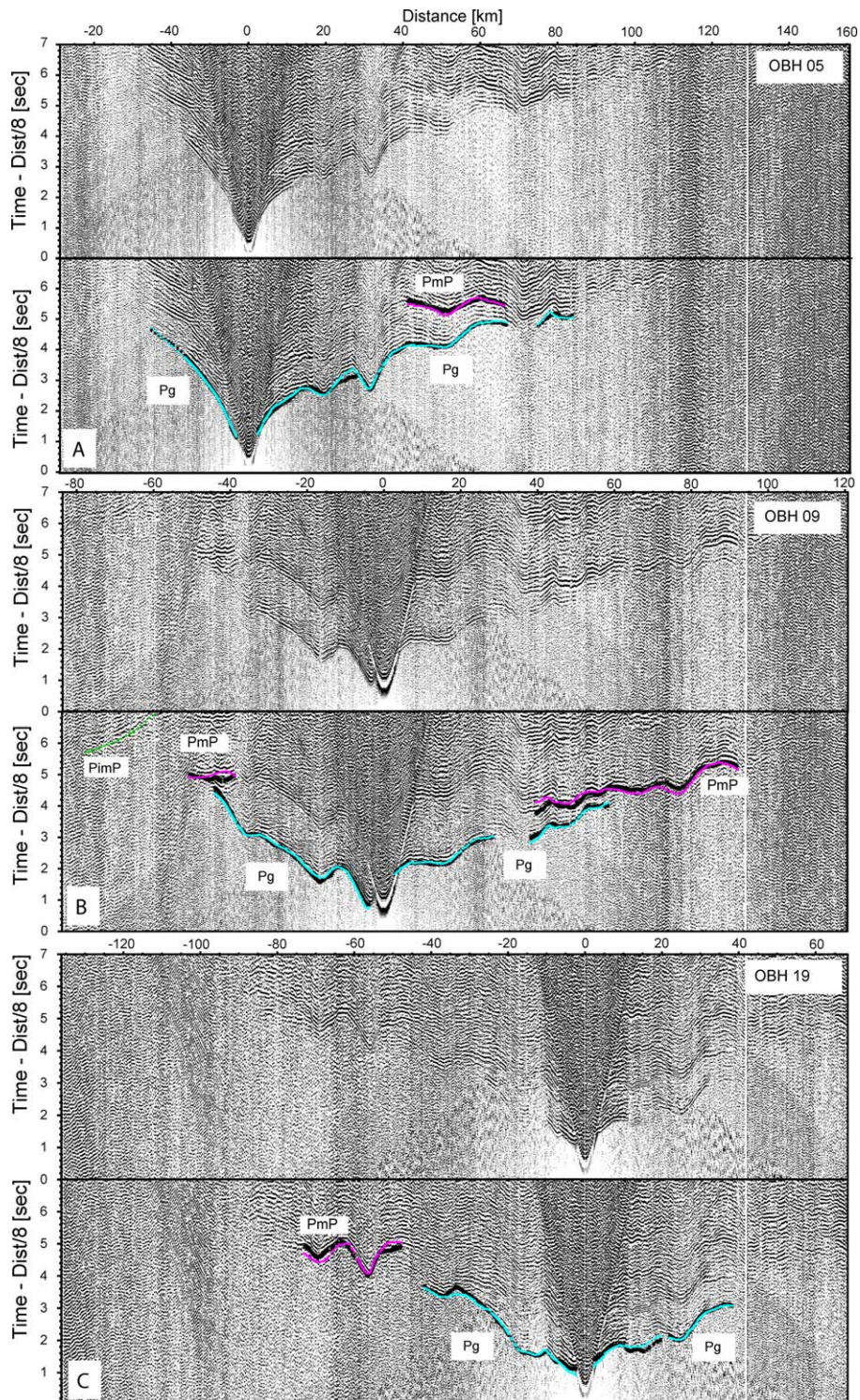
Figure 2. Examples of record sections: (a) OBH03 is located at the Corsica Basin (98 km). Slow arrivals of Pg phases indicate a thick sediment infill of the basin. (b) OBH09 east of Corsica Basin (150 km). Velocities are faster in the east then in the west. PmP arrivals are observed over 40–60 km offset range. (c) OBH19 at the eastern end of the profile (237 km). Black = picked arrivals; purple, cyan, and green = inverted arrivals.

bottom and vertical correlation lengths ranged from 0.75 to 2 km respectively. For velocities and depth, smoothing and damping weights were kept fixed for all phases with 170/20 and 30/20, respectively [*Korenaga et al.* 2000]. A weighting factor of $w = 1$ was used to invert for
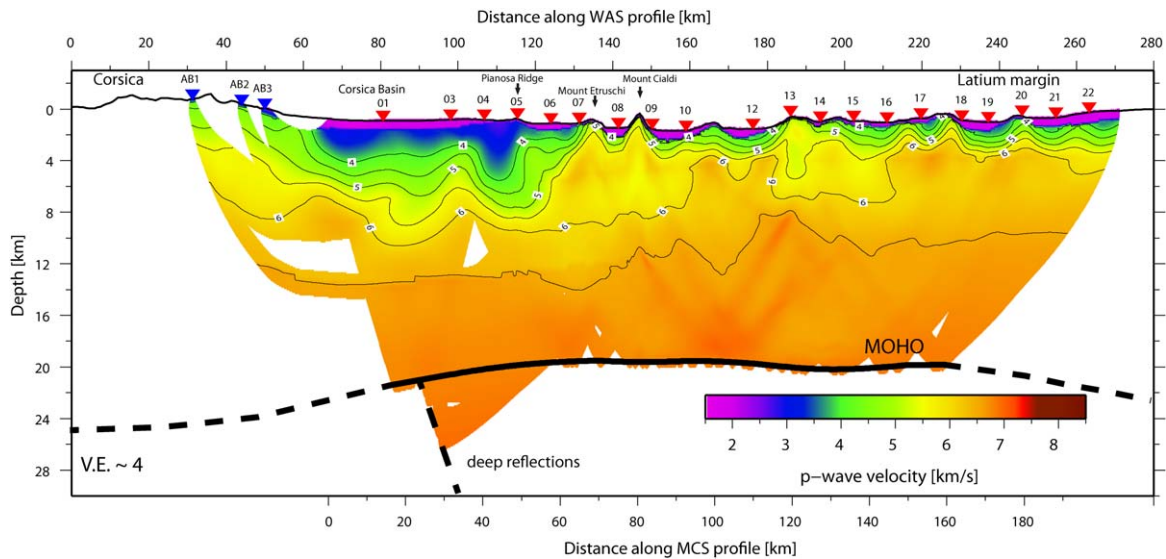
Figure 3. The final result of the *p* wave tomography along the MEDOC-AB line reveals the architecture of the crust and the crustal thickness. The section can be divided in two domains: (1) the Corsica Basin to the west bounded by the Pianosa Ridge to the East and (2) a series of fault-bounded horsts and grabens toward the Latium Margin.

the depth and velocity nodes equally. In the last inversion step all Pg-phases were jointly inverted with the PmP-arrivals to determine the geometry of the Moho. Late reflections (PimP) observed on OBH06–10 were included in a later inversion step, because the code does not allow for inversion of multiple floating reflectors. We first inverted for all Pg- and PmP-phases, kept the final crustal model fixed and inverted for the deep arrivals afterward. Figure 3 shows the crustal velocity model of the final inversion result.

3.2.2. Multichannel Seismic Data

[14] The MCS data of profile A-B were processed using the software package OMEGA2 (Western-Geco). Focusing analysis, velocity model building and prestack depth migration were carried out with SIRIUS (GX-Technology). The processing steps were: setting geometry and the subsequent calculation of CMP locations on a crooked line, predictive deconvolution, prediction of multiples using the propagating wavefield followed by adaptive subtraction, sorting into CMP-gathers, initial velocity analysis using focusing analysis and iterative prestack depth migration based on the Kirchhoff integral solution. Afterward, primary events were overcorrected and an FK-filter (frequency-wavenumber) and time-variant band-pass filter were applied. In the last step focusing analysis was carried out again to achieve a final velocity field for the sedimentary and upper crustal structures. Velocities in the deeper part of the crust cannot be obtained from the MCS data itself and

were therefore supplemented by the velocities from the wide-angle inversion result. The final result is the prestack depth migrated seismic section (PSDM) shown in Figure 7. For the prestack time section the velocity field in depth was transformed to two-way travel time and then used for time migration.

4. Results

4.1. *p* Wave Velocity Model

[15] Modeling of the WAS data resulted in the crustal velocity structure shown in Figure 3. The last inversion, including all phases, resulted in a misfit of 81 ms and $X^2 = 2.1$ after eight iterations. Pg phases had a misfit of 54 ms and PmP phases of 123 ms. The inversion of additional deeper reflections (PimP) results in a larger misfit of 230 ms and is therefore only discussed qualitatively. The major feature in this profile is the ∼60 km wide and ∼6–7 km deep Corsica Basin. Here Vp increases from 1.8 km/s at the seafloor to 2.5 km/s at a depth of 1.5 km, further to 3.5 km/s at a depth of 3 km (Figure 4). The basement of the basin is located at a depth of 6–6.5 km with a Vp of 6 km/s.

[16] At the eastern rim, near the position of OBH05, the Corsica Basin is bounded to the east by the Pianosa Ridge at km 115 in the model (Figure 3). Here a narrow area shows lower velocities
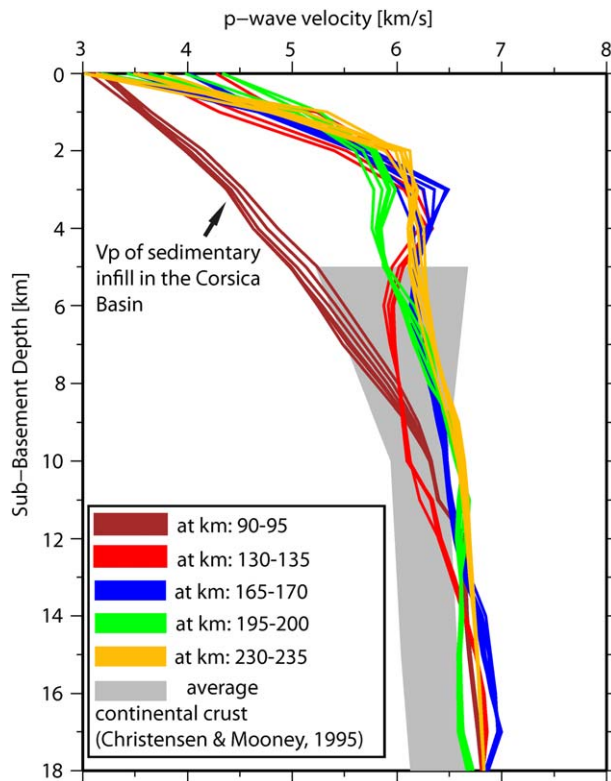
Figure 4. 1-D velocity profiles extracted from the tomographic inversion result. Vp between 130 and 235 km are compared with the average global velocities in continental crust published by *Christensen and Mooney* [1995]. Vp shown for the Corsica Basin (90–95 km) start at Top-Messinian (Y).

increase rapidly from 3.5–4.0 km/s to 5.5 km/s at a depth of ~2 km below basement (Figures 3 and 4).

[18] In the middle part of the crust, velocities increase from 5.5 to 6.0 km/s at a depth of 4–5 km below basement, but in two areas between km 160 and 180 and between 210 and 260 km, they increase to 6 km/s at a depth of 3 km below basement. The lower part of the crust has velocities between ~6.0 and 6.8 km/s. 1-D profiles extracted from 5 km wide portions of the model show that velocity in the middle crust (5–9 km below basement) is representative of typical continental crust (Figure 4). Vp values in the lower crust of 6.8 km/s are ~0.3 km/s faster than the average continental crust [*Christensen and Mooney*, 1995]. The inversion of PmP-phases reveals a crystalline-crustal thickness varying from ~15 km beneath the sedimentary infill of the Corsica Basin to ~17 km beneath the N-S trending ridge structures east of the Corsica Basin. Except for some minor undulations, the Moho shows no variation in depth.

4.1.1. Model Resolution and Uncertainties

[19] To find model uncertainties and check the robustness of the final model we produced a range of starting models by modifying the velocity field by ± 5%, crustal thicknesses by ± 1, 2, and 3 km and combinations of all parameters. We found that nearly all perturbed starting models evolve toward the final preferred model (Figure 5c). Hence, the model is robust. Statistical calculations [*Korenaga et al.*, 2000] yield the standard deviation for velocities and the uncertainty width for the Moho location (Figure 5b).

[20] The uncertainties in the upper crustal domain are about 0.1–0.15 km/s except for some outliers (Figure 5b). Velocities in the Corsica Basin are well determined (<0.1 km/s) although the ray density is less than in the eastern upper crust. Just beneath OBH03 at 8 km depth, the uncertainty grows to 0.2 km/s due to less dense ray coverage. In the middle and lower crust, *p* wave uncertainties are 0.1–0.2 km/s. Figure 5a shows the derivative weight sum (DWS), which is a measurement of ray density passing each cell. From the ray density, we infer that the upper and middle crust between km 120 and 220 is well covered by rays. Furthermore, the DWS indicates that velocities in the middle and lower crust are mainly constrained by ray paths of PmP reflections and thus are not as dense as those covered by rays as in the upper crust. We carried out a resolution test of our section by adding a checkerboard pattern with high and low velocity cells of 10 km width and 5 km

of 3–3.5 km/s compared to the surrounding velocities of 4–4.5 km/s. In this zone, the seismic records (OBH03-OBH09) show that the amplitude of first arrivals diminishes and that the apparent *p* wave velocities decrease. This can be seen for instance at ~40 km offset on OBH09 (Figure 2). The western rim of the basin, near the coast, is poorly constrained due to a gap of shots and receivers.

[17] For the inversion of the late PimP phases, we attempted to invert for a steep dipping reflector underneath the Corsica Basin. We also tried to invert for a flat reflector within the mantle, but the inversion process shifted the reflector back to a steep and eastward dipping reflector. However, the actual geometry could not be resolved by the data. East of the Corsica Basin/Montecristo Basin, a series of horst and graben structures continues toward the Latium Margin. The sedimentary cover and the basin infill have velocities of 1.8–2.0 km/s in agreement with velocities obtained by focusing analysis of MCS data. The inversion result shows the block structures along the profile in horizontal and vertical extent. Velocities underneath the sedimentary cover
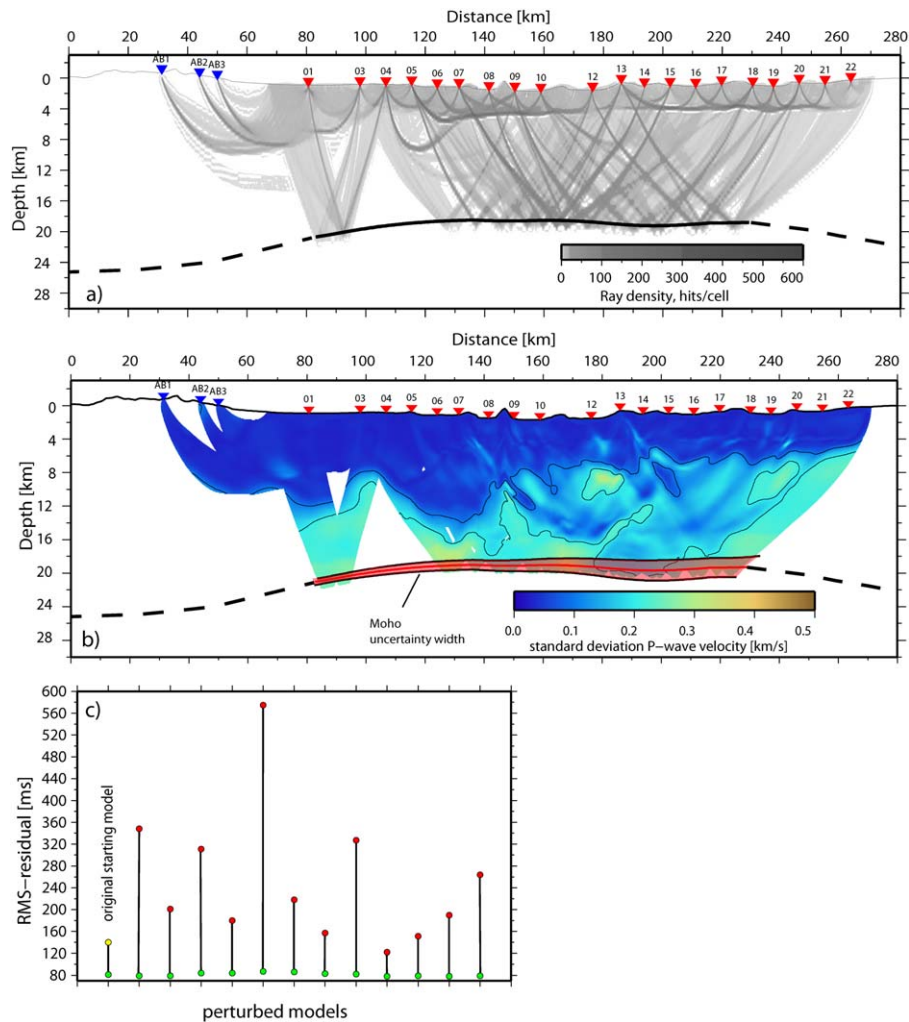
Figure 5. (a) Ray density (DWS), (b) standard deviation for *p* wave velocities derived by the inversion of perturbed starting models. (c) RMS residuals for perturbed starting models. Red dot indicates the residual at the start of inversion. Green dots mark the residual after the last iteration. All perturbed models evolve close to the final model of the original starting model (yellow dot).

height. The velocity perturbation was ± 10%. The checkerboard resolution test reveals that the upper crust and the Corsica Basin are well resolved. In the middle and lower crust, the resolution decreases (Figure 6).

4.2. Tectonic Structure and Sediment Deposits

[21] The prestack depth-migrated image is shown in Figure 7 and overlain with the final tomographic wide-angle velocity model of Figure 3 to show the good correlation of the different features depicted by both data sets, including the sedimentary units and crystalline basement. The sedimentary units in the Tyrrhenian basin have been studied by many

authors (e.g., *Zitellini et al.* [1986], *Trincardi and Zitellini* [1987], and *Sartori et al.* [2004], among others).

[22] The start and end of the rifting is associated with two regional unconformities: the "L" unconformity, which is late Tortonian in age and the "X" unconformity, which is Early-Pliocene in age [*Trincardi and Zitellini*, 1987]. Between these two unconformities the "Y" unconformity marks the top of the Messinian sequences. In the Corsica Basin and northernmost part of the Tyrrhenian Sea sediment units are calibrated with two exploratory wells [*Mauffret et al.*, 1999]. In addition, scientific drilling was carried out in the 1980s (Ocean Drilling Program (ODP) leg 107) on a NW-SE transect (Figure 3). Although, the Site 654 of ODP leg 107
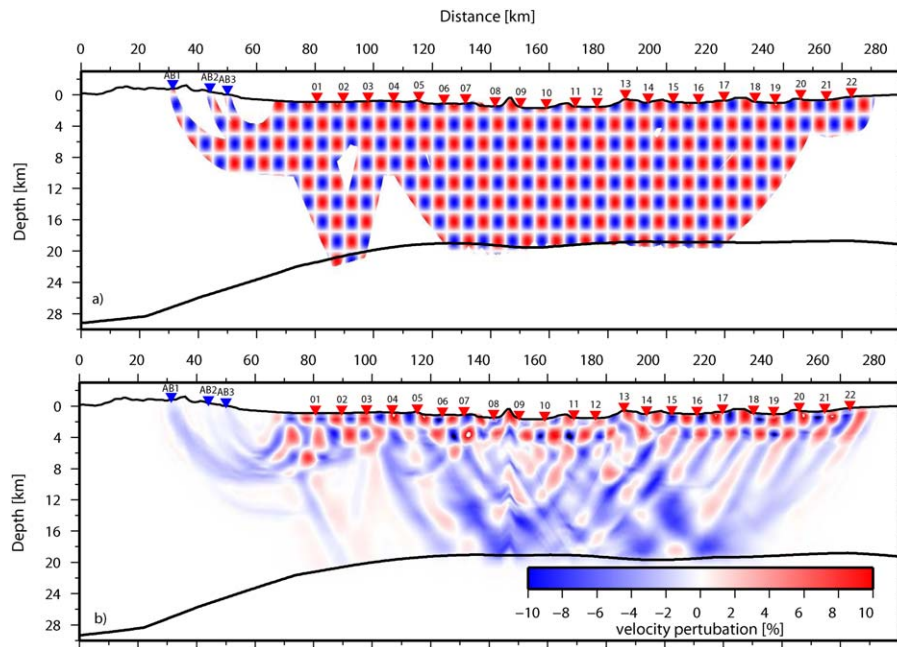
Figure 6. (a) Checkerboard test: Velocity perturbations of 10% with wavelength of 5 km × 10 km were added to the data. (b) The recovery shows that the upper crust and the deeper parts of the Corsica Basin are well recovered.

(Figure 1) is located ∼100 km further south, it supports our age interpretation of the seismic units [*Kastens et al.*, 1988].

4.2.1. Corsica Basin

[23] The PSDM image (Figure 7) shows well-imaged sedimentary units of the Corsica Basin above the basement at 6.0–6.5 km depth (5 s two-way-traveltime). The top basement depth is in good agreement with the tomographic model, where we observe velocities of ∼5.5–6.0 km/s (Figures 3 and 7). Toward the east, the basin becomes thinner and is bounded by several westward dipping reflectors at the Pianosa Ridge. The youngest sedimentary unit (Early-Pliocene to Holocene) in the basin is ∼600 m thick and thins to ∼250 m toward the east. Sediments are subhorizontal with velocities of 1.8–2.0 km/s. A high amplitude reflector below, is identified as the "Y" Messinian reflection (Figure 8), indicating that the sediments above are Pliocene to Quaternary in age. However, the "X" reflector of Early-Pliocene age [*Trincardi and Zitellini*, 1987] is difficult to identify within the basin. The sequence is undisturbed and shows no evidence of major tectonic activity.

[24] The end of the Messinian depositional sequence is marked by a prominent reflection beneath the transparent and younger basin infill and can be observed along the complete seismic profile ("Y" in Figure 8). At places, the Top-Messinian in the Corsica Basin is an erosional unconformity that is intersected by drainage canyon structures [*Mauffret et al.*, 1999, *Zitellini et al.*, 1986]. Furthermore, this reflector is tilted, dipping toward the west.

[25] In the upper part of the ∼800 m thick Messinian unit (Figure 8), the layering is more or less undisturbed. However, it is slightly deformed in the lower part of the unit, which is characterized by a succession of thin and discontinuous reflectors. Velocities in the Messinian unit increase with depth from 2.5 to 3.5 km/s. Below the Messinian units another high-amplitude reflection marks the top of Langhian deposits [*Mauffret et al.*, 1999] followed by a succession of several thick layers. The top Langhian horizon shallows from a depth of 2500 m in the west to 1000 m depth in the east. Velocities increase with depth from ∼3.5 to 5.5–6.0 km/s. At the Pianosa Ridge Langhian and pre-Langhian sediments terminate against the westward dipping unit (Figures 7 and 8). This area is marked by a large and prominent Vp-anomaly of 2.5–3.5 km/s that is clearly observed in our WAS data at 115 km (Figures 3 and 8).

4.2.2. Fault-Bounded Blocks and Sedimentary Basins

[26] East of the Corsica Basin a series of blocks (A1-A10 in Figure 7) separated by sedimentary
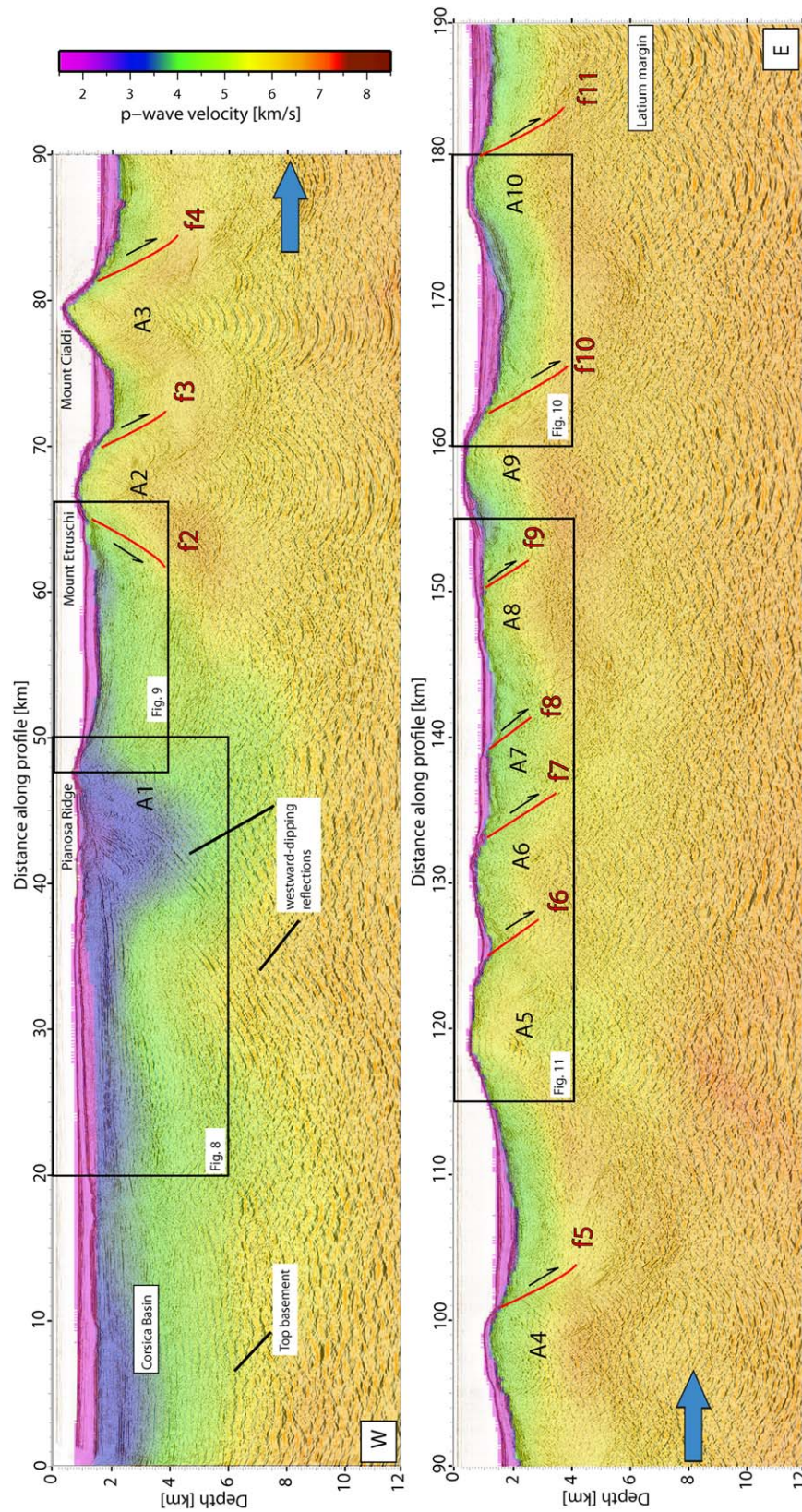
Figure 7. Prestack depth migrated section overlain with the velocities obtained from the tomographic inversion of WAS data. The basement of the Corsica Basin is located at 6–6.5 km depth and bounded to the east by westward dipping reflections. East of the Corsica Basin the main faults f2–f11 bound large rotated basement blocks (A1–A10) toward the Latium Margin.
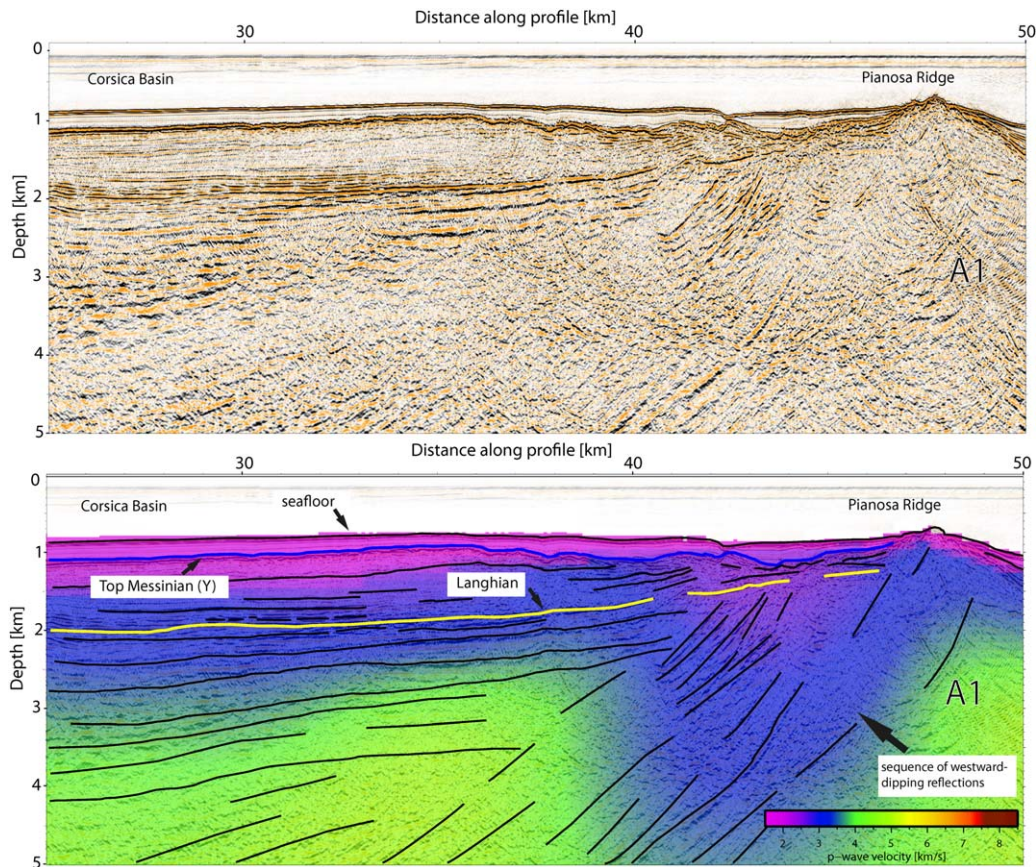
Figure 8. The sedimentary structures in the Corsica Basin terminate against westward dipping reflectors which can be observed in the seismic data to a depth of at least 10 km depth. p wave velocities in the upper part of this complex are reduced to 2.5–3.5 km/s and indicate higher fracturing. See Figure 7 for location.

basins extends onto the Latium Margin. The structures are also seen in the bathymetry data where the sediment cover is thin. Major faults

Table 1. Extension Factor β_f Calculated by the Measured Dips of the Main Faults (f2–f11) and Rotated Basements of the Hanging Walls[a]

Major Fault	Fault Dip α [°] ±5°	Basement Dip θ [°] ±2°	Initial Fault Angle $(\alpha + \theta)$ [°]	$\beta_f/-(\alpha)$, $+(\theta)/+(\alpha),-(\theta)$
f2	40	10	50	1.19/1.27/1.13
f3	50	25	75	1.26/1.34/1.19
f4	40	11	51	1.26/1.29/1.14
f5	40	10	50	1.19/1.27/1.13
f6	31	14	45	1.37/1.52/1.26
f7	38	11	49	1.28/1.32/1.16
f8	30	10	40	1.28/1.42/1.19
f9	30	12	42	1.33/1.48/1.23
f10	30	10	40	1.28/1.42/1.19
f11	38	10	48	1.26/1.29/1.14
				$\varnothing = 1.27$ $+ 0.09/-0.10$

[a]The sum of these angles is assumed to be the initial fault angle. Maximum uncertainties for β_f occur for negative and positive combinations of the estimated uncertainties for faults and basement dips.

(f2–f11) are clear in the PSDM section to a depth of 3–4 km and are apparently not linked at depth. The general observation is that the blocks rotated on eastward dipping and major faults (synthetic faults). This led to the formation of half-grabens with syn-tectonic and prerift structures dipping westward. Fault dips vary between 25° and 50° (Table 1 and Figure 11) and lower syn-tectonic deposits are tilted 10°–25°. An exception is the block A2 (Mount Etruschi), which is bounded by the faults f2 and f3 (Figure 7). The adjacent blocks A3–A10 are bounded by faults dipping 30°–40°. The size of the blocks decreases from A5 to A7 toward the east and block A8 is fractured by a set of smaller synthetic and antithetic faults dipping ~30° (Figure 11). Blocks A9 and A10 are larger and separated by fault f10.

[27] The sediment infill can be divided into three main units. (1) The horizontally deposited and undeformed sediment sequence of Early-Pliocene to Quaternary age with a thickness of 200–600 m;
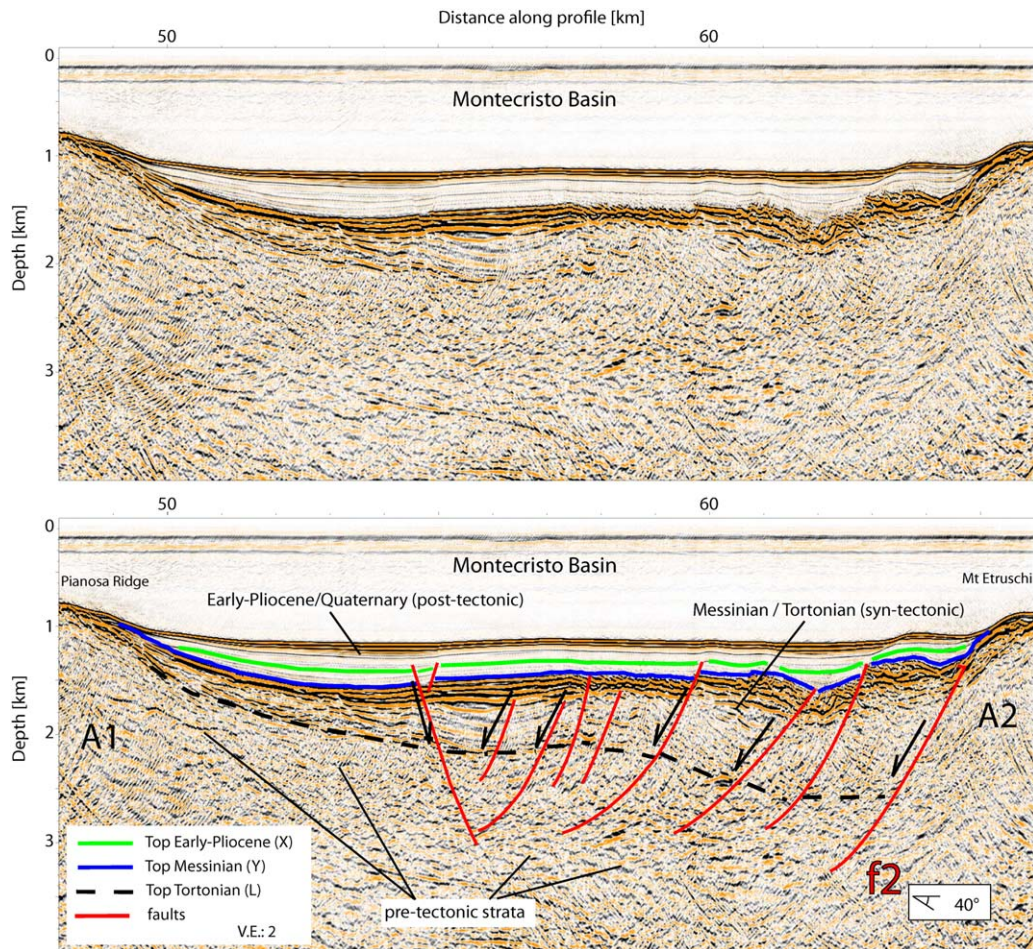
Figure 9. The sedimentary infill of the Montecristo Basin shows that tectonic activity mainly took place during Early-Pliocene (X) to Tortonian age (L). This fan-shaped syn-tectonic sequence is cut by normal faults and overlain by undisturbed Early-Pliocene to Quaternary sediments. Weak reflections within the crust are interpreted as pre-tectonic strata. See Figure 7 for location.

(2) the end of Messinian to Early-Pliocene unit with amplitudes similar to the sequence above but cut by small faults; and (3) the Messinian and Tortonian successions that can be traced throughout the entire section, typically abutting block-bounding faults and internally cut by small normal faults. Below the stratified Messinian-Tortonian sequence, a domain with less stratified reflectivity can be interpreted as the basement. Reflections within the basement are weak and in many places absent.

[28] The different sedimentary units are well imaged in the Montecristo Basin (Figure 9) located between block A1 (Pianosa Ridge) and A2 (Mount Etruschi). Here the Early-Pliocene to Quaternary unit marks the post-rift sedimentation. Like in the Corsica Basin, the top of the Messinian

deposits is marked by a high-amplitude reflector. Across the basin, the Messinian unit is cut by normal faults forming small tilted blocks. Its internal structure is chaotic in the eastern segment, wavy or folded possibly by slumping (e.g., at the top of block A6 in Figure 11). Tilted Messinian strata indicate that the main rift phase occurred during this age. The shape of the syn-tectonic sequence in the Montecristo Basin (Figure 9) is fan shaped but at other sites it has rather constant thickness and seems to be uplifted or onlapping on the footwall. At the Latium Margin between blocks A9 and A10 the Messinian deposits are fan shaped near the footwall, but lying stratified on the hanging wall (Figure 10).

[29] Extension, which is generated by the fault displacements that occurs along the profile, varies
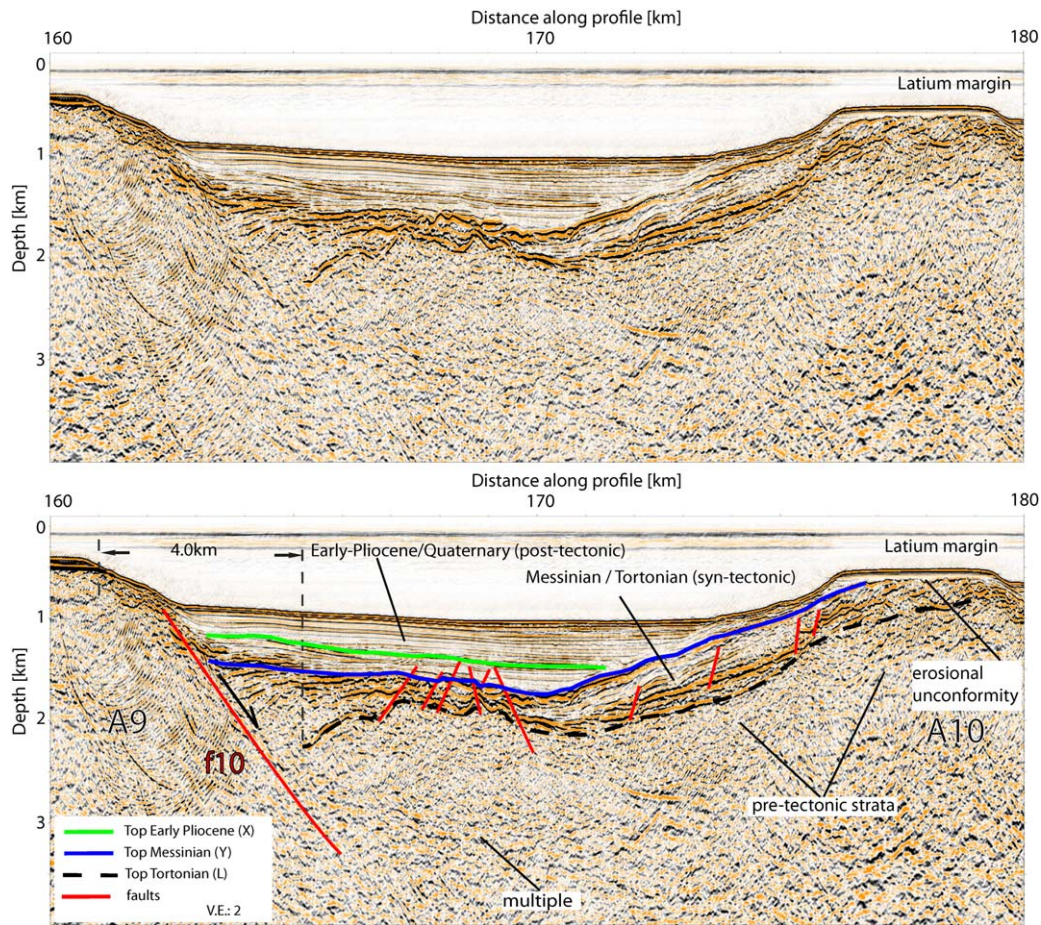
Figure 10. The syn-tectonic sequence near the Latium Margin forms a fan-shaped geometry at the footwall of block A9 and is stratified deposited on top of the hanging wall of A10. The flat summits and the unconformity on top of block A10 indicate that during the active rift phase the Latium Margin was above sea level and subsided when rifting stopped. See Figure 7 for location.

between a few hundred meters (e.g., f2) and several kilometers, for instance the pre-tectonic basement of block A9 and A10 (Figure 10).

5. Estimating Horizontal Extension

[30] To determine the amount of extension we made several assumptions: (a) the dip of the faults on the PSDM section is the true angle, because the seismic section is orientated perpendicular to the horst and graben structures. Hence, the fault angle and the length of the pre-tectonic crust in the seismic data will be accurate. (b) We assumed that faults are planar and that the angle can therefore be measured directly. (c) The top of the pre-tectonic crust of Tortonian age is the base of the continuous strata of the Messinian deposits assuming it marks an isochrone. Hence, horizontal extension is the difference of the current profile length to the

pre-tectonic crustal length or, alternatively, the sum of fault offsets produced by all faults. (d) For domino-like rotated blocks the relative extension β_f can also be calculated by the fault dip (α) and the rotation of the bed (θ) by the following expression [*Wernicke and Burchfiel*, 1982]:

$$\beta_f = \sin (\alpha + \theta)/\sin(\alpha) \qquad (1)$$

[31] We applied two different methods to determine the amount of horizontal extension based on assumption (c) and (d). In the first approach, we estimated the ratio of the length of the pre-rift basement to the actual profile length to obtain β_{pb} (Figure 11). In a second method we used the dips of the major faults and tilted strata of the hanging wall to determine a relative extension factor β_f by using equation (1). We excluded the Corsica Basin and westward dipping reflectors between km 0 and km 48. The Corsica Basin formed during an
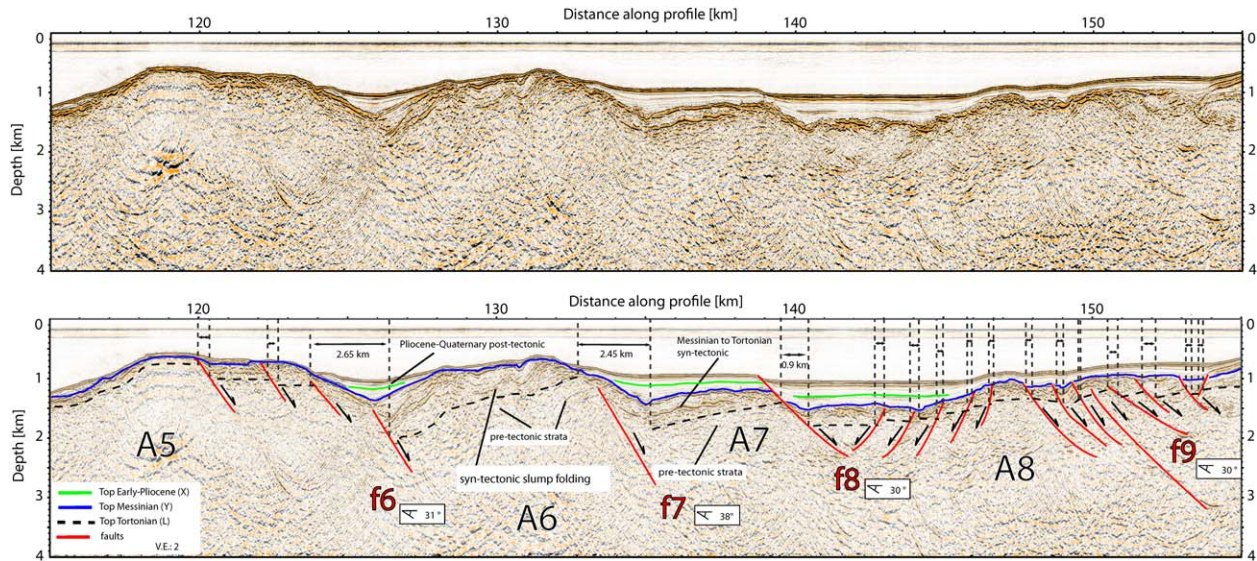
Figure 11. Closeup of MCS section from Figure 7. The vertical dashed lines show the horizontal component of space accommodated by the heave of normal faults. Thick dashed lines indicate the base of the stratified syn-tectonic sequences of Messinian age that is interpreted as the top of the basement.

earlier rift stage that is coeval with the development of the Ligurian-Provencal basin during the Oligocene-Early Miocene [*Mauffret et al.*, 1999]. In addition, there is only minor evidence for tectonic activity in Messinian to Langhian (16 Ma) sediments within the Corsica Basin, showing that the basin was not affected by the main Tyrrhenian rift phase.

[32] Table 1 lists the measured fault dips (α) of the faults f2–f11 bounding the largest blocks and the rotation angle of the top of basement (θ) of the hanging blocks. Nearly all faults dip $\sim$30°–40° and the base of the syn-tectonic/pre-tectonic successions are tilted 10°–15°. The error of the fault dip estimation is $\pm$5°. For the estimation of the rotated basement dip, we estimate an error of $\pm$2°. The maximum error with equation (1) occurs for asymmetric uncertainty combinations (Table 1). The average result for β_f is then $1.27 + 0.09/ -0.10$.

[33] By quantifying the length of the crust in the hanging wall we included the displacements of all faults identified in the seismic section. As an example, the interpretation of the segment between km 115 and km 155 shows the Early-Pliocene-Quaternary post-tectonic deposits and the Messinian/Tortonian syn-tectonic sequence (Figure 11). The black dashed line indicates the assumed and measured pre-tectonic basement. Toward the east the measurements stop at block A10 (180 km) because the next block is not fully

imaged (Figure 7). Thus, the profile length considered is 132 km. The length of the basement adds up to 101 km, resulting in an extension factor (β_{pb}) of 1.3 or 30%. This result is very close to the relative extension factor (β_f) of 1.27, or 27%, produced by the main faults. Hence, the opening rates of the basin in this area can be calculated to 7.8–10.3 mm/a assuming an active rift phase of 3–4 Ma.

6. Discussion

6.1. Crustal Structure and Thinning

[34] The velocity structure and thickness of the crust is obtained by inversion of the WAS data (Figure 3). The tomographic inversion yields a $\sim$15 $\pm$ 1 km thick crystalline crust under the Corsica Basin and a $\sim$6 km thick sedimentary infill. The Bouger-anomaly map shows values of +10 mGal in this area (Figure 1b). Beneath the horst and graben structures a 17 $\pm$ 1 km thick crust has been revealed. The crustal thickness shows no significant variation in agreement with the gravity field of +70 mGal (Figure 1b).

[35] A SW-NE receiver function transect obtained from teleseismically recorded earthquakes, found a 25 $\pm$ 1 km thick crust under northern Corsica that thins to 20 $\pm$ 2 km toward the Tuscany margin and increases to $\sim$50 km under the northern
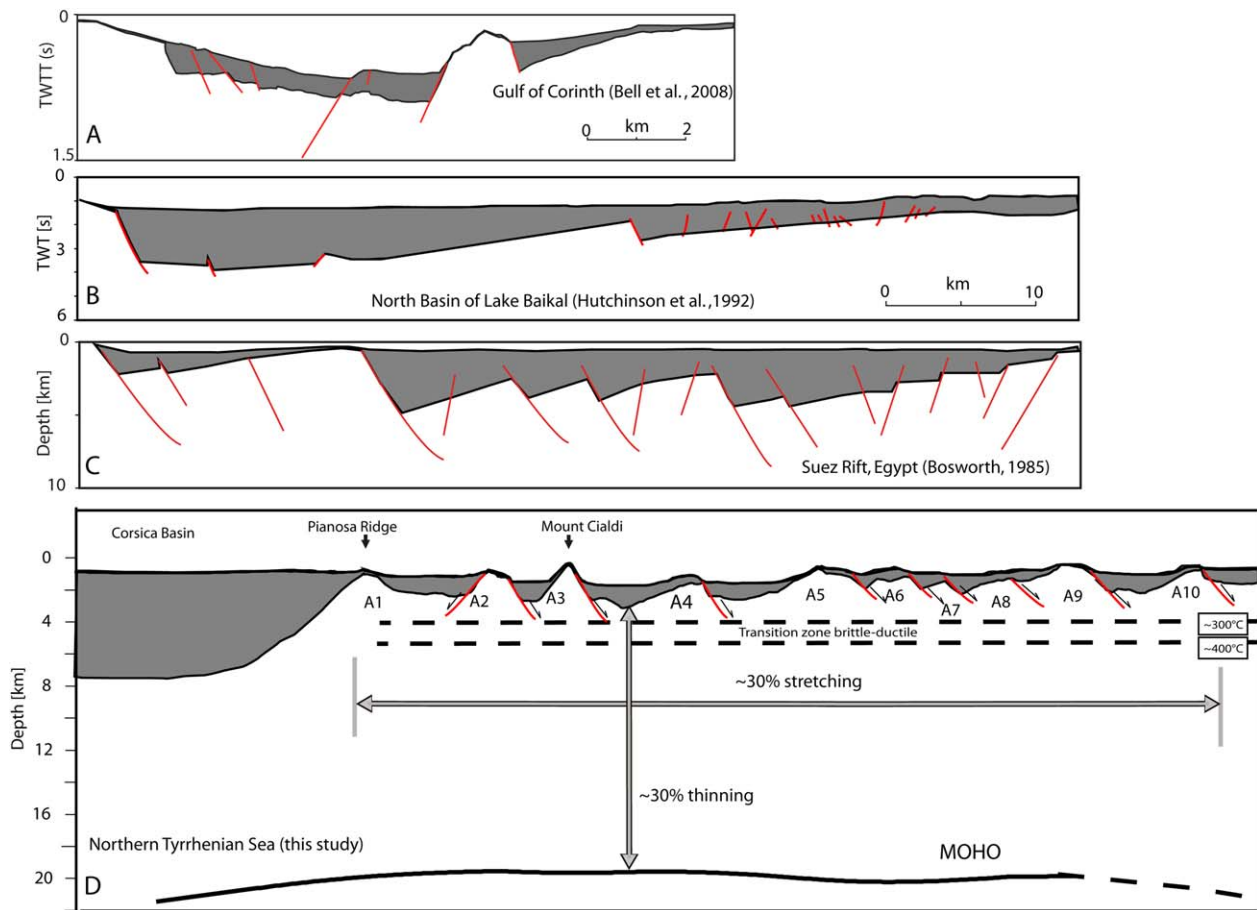
Figure 12. Structural comparison of seismic cross sections from other young rift settings (A–C) with the seismic cross section presented here (after Bell et al., 2008; Hutchinson et al., 1992; Bosworth, 1985). Grey colored areas indicate sedimentary deposits. Half-graben formation and asymmetry seem to be a general feature of rifts. (d) East of the Corsica Basin the crust is stretched by 30% which is equal to the amount of crustal thinning. Heat flow data and thermal gradients are from *Della Vedova et al.* [1984].

Apennines [*Mele and Sandvol*, 2003]. *Contrucci et al.* [2005] modeled marine shots recorded on land ∼50 km north of the profile (line LISA-10 in Figure 1). They found a 15 km thick crust under the Corsica Basin and a 23–25 km thick crust between Pianosa Ridge and the Tuscany Margin. Along our transect, the crust is also 15 km thick under the Corsica Basin and is 17 ± 1 km thick east of Pianosa Ridge. This comparatively thinner crust (17 ± 1 km) indicates a more intense period of stretching toward the south.

[36] Assuming that the 17 ± 1 km crust originally had an initial thickness comparable to current Corsican crust (∼24 km) implies a thinning factor β_v of ∼0.70 (∼30%). The factor β_v is correct only if the crust has not modified by magmatic additions. The tomographic inversion (Figure 3) shows, that the lower crust is fairly homogeneous eastward of 115 km without high-velocity anomalies that

might indicate important magmatic intrusions. However, velocity-depth profiles from four different locations along the profile (Figure 4) display typical continental crust values in the upper crust (upper ∼8 km of basement) but with slightly higher values in the lower crust of 6.6–6.8 km/s compared to average continental crust [*Christensen and Mooney*, 1995]. These velocities probably indicate a higher-than-average percentage of mafic minerals but they are still not evidence for large-scale intrusive magmatism.

[37] Nevertheless, the deep wide-angle reflections under Corsica Basin, recorded on OBH06–10, might indicate magmatic intrusions in the upper mantle. The Corsica Basin is bordered to the east by a curved band of high-amplitude magnetic anomalies of 120–160 nT (Figure1c) that might be related to magmatic intrusions. This band extends from west of Elba Island to Pianosa Island and

along the Pianosa and Montecristo Ridges to the southwest. The profile crosses Pianosa Ridge where the anomaly has decreased amplitude. Here velocities range between 3.5 and 5 km/s at a depth of 10 km, which are possibly too slow for a magmatic intrusions related to rifting.

[38] However, the source of magnetic anomalies might have a deeper origin, perhaps from the mantle where the PimP-reflection originates. Similar reflections occur at the same depth near Elba Island [*Ponziani et al.*, 1995] in the area of high magnetic anomalies. This suggests that the late reflections might originate from an intrusive structure, even though they could have been recorded as side reflections from shallower structures. A positive gravity anomaly just south of the profile is coincident with a magnetic anomaly and might support the existence of an intrusive feature (Figures 1b and 1c).

[39] The west-dipping sediment unit at the eastern edge of the Corsica Basin might be related to thrusting formed during the collisional phase between Corsica-Sardinia and the Apulian continental block [*Keller and Coward*, 1996]. *Mauffret et al.* [1999] propose that the basin formed over a collisional prism in a forearc position between Corsica and the Adriatic plate, and that the thrusts are Alpine. Our inversion of WAS data reveal that this area has reduced velocities of 2.5–3.5 km/s in the upper 5 km, which may indicate a highly fractured region (Figure 8). Alpine thrusts might represent an inherited structure that mechanically decoupled the Corsica Basin from the crust in the east.

6.2. Style of Extension

[40] The rifted continental crust between the Pianosa Ridge and the eastern Latium Margin is characterized by continental half-graben structures. PSDM images show that the blocks are bounded by normal faults that accommodate space in the upper crust.

[41] The geometry of syn-tectonic strata reveals the sense of block rotation, dip-angle of bounding faults and helps to recognize the rotated top of the basement. We found that nearly all major faults dip at angles of 30–40° to the east. The respective dip of the pre-tectonic strata at the hanging walls (base of the syn-tectonic deposits) ranges from 10°–15°. The only exception is block A2 (Figure 7). The faults bounding this block dip at angles of 40° (f2) to the west and 50° to east (f3). We therefore interpreted that Mount Cialdi (A3) rotated on

f3 and the block A4 on the fault f4. This is supported by the thickening geometry of syn-tectonic deposits in the half-graben east of the block A3 (Figure 7). Thus, it is reasonable to deduce that the western flank of A3 forms the top of the basement. The rotation direction of A2 (Mount Etruschi) is not clear in the images. Syn-tectonic deposits indicate that block A1 and the basement of Montecristo basin tilted westward on the fault f2. This is inferred from fan-shaped eastward thickening of syn-tectonic strata (Figure 9). The adjacent blocks A3–A5 are bounded by faults dipping 30°–40°. The Messinian deposits seem to be uplifted in the vicinity of the footwall of blocks A3 and A4 (Figure 7) or lying stably on the flank of the hanging wall of block A10 (Figure 10). A possible explanation for this sedimentary architecture is that the stress field was not exactly orientated W-E during part of the rifting process and had a strike-slip component which led to oblique faulting. Furthermore, the syn-tectonic deposits are of similar thicknesses and ages, from which we infer that the faults were active and rotated mainly during the Messinian.

[42] At 120–140 km, the dip of the faults bounding blocks A6 and A7 is 31° and 38°, respectively. The top of basement dip of A6 is steeper than of A7 (14° and 11°) and the syn-rift deposits thicker on top of A6. This might be an indication for eastward propagation of fault activity.

[43] Block A8 is cut by a set of small synthetic and antithetic faults dipping ∼30° either west or east and contributing to the total extension with small displacements (Figure 11).

[44] Block A9 and A10 are comparatively larger and separated by the fault f10 (Figure 10). The top of the blocks A9 and A10 may have been above sea level during the Messinian salinity crisis and are relatively flat, probably cut by wave erosion. Wave base erosion is inferred from the erosional unconformity truncating syn-tectonic strata on the summit of block A10 (Figure 10). The thicker syn-tectonic deposits between A9 and A10 may be the eroded material from the top of the blocks (Figure 10). Block A9 is in fact a ∼20 km long NW-SE orientated extended plateau with a maximum width of 5 km (Figure 1) that probably belong to a former shelf region.

[45] We found that the space accommodated by the main faults (f2–f11) is on average 27% ($\beta_f = 1.27$). By estimating the pre-tectonic length using the top of the basement as a marker horizon

and including all seismically imaged faults, we found a stretch factor (β_{pb}) of 1.3 (30%). The minor difference of β_f and β_{pb} shows that the space accommodated in this rift is mainly localized by the heaves of large surface-breaking faults and implies that smaller faults within the hanging walls do not significantly contribute to the entire stretching.

6.3. Comparison with Other Rifts

6.3.1. Half-Graben Formation

[46] The northern Tyrrhenian Basin opened due to the formation of 10 major east-dipping offshore faults that generated crustal extension and led to the formation of half-graben structures (Figures 7 and 12). Thus, the fault vergence of the major normal faults in this early rift stage appears to be different to the conceptual pure-shear model [e.g., *McKenzie*, 1978]. Hence, the upper crustal tectonic structure in the rift appears asymmetric, sharing similarities with observations from other young continental rifts.

[47] Asymmetric fault block structure has been described at the western Gulf of Corinth [*Bell et al.*, 2008], the Galicia interior Basin [*Pérez-Gussinyé et al.*, 2003], the intracontinental Baikal rift [*Hutchinson et al.*, 1992] and the Upper Rhine Graben [*Derer, et al.*, 2005]. Detailed field work has characterized asymmetric half-graben structures at the Hammam-Faraun block of the Suez Rift. From this rift, it has been shown that the active block-bounding major faults formed after the onset of rifting, and that smaller intrablock faults are older but abandoned with time [*Gawthorpe et al.*, 2003]. Subsequent fault displacement was localized during the development of the major fault systems. Localization is similar to the observations on the image presented of the northern Tyrrhenian Sea.

[48] The study on the Hammam-Faraun fault block further shows, that the major faults formed sequentially in time. From the PSDM image, we have no evidence of the relative age of smaller faults within fault blocks and the major fault system bounding them. Thus, it remains uncertain whether the smaller faults are older or are coeval to block deformation. In a model that explains rift structures of the West Iberia and Newfoundland conjugate margins it is proposed that individual successive faults cut crust that had been previously extended by earlier individual faults [*Ranero and Perez-Gussinye*, 2010]. We point out that the series of tilted blocks A5–A7 may have undergone a

similar development because the dimensions of the half-grabens and block size diminish toward the east (Figure 11).

6.3.2. Fault Initiation and Thermal State

[49] The major faults imaged on the PSDM dip 30°–40° and the hanging wall is rotated ~12° (Table 1). This suggests that the initial fault angles were approximately ~45°–50°. This angle is smaller than for an optimally orientated high-angle normal fault that initially dips at ~65° with coefficients of friction of 0.6–0.85 [*Abers*, 2009]. Early rift faults, like at the Suez Rift [*Gawthorpe et al.*, 2003], exhibit major faults dipping 60°–80° in their shallower segments. However, earthquakes at extensional settings, for instance in the Gulf of Corinth rift, show that the majority of large events nucleate on normal faults that dip 40°–50° [*Jackson*, 1987]. This observation supports the notion that major faults in the northern Tyrrhenian may have initiated at this angle. However, this estimation contains considerable uncertainty. This is because the scarcity of well-imaged prerift strata that may have been deposited horizontally precludes an accurate estimate.

[50] The initiation angle of the faults is dependent upon the rheological state of the crust. If the crust is weak, faults might initiate at shallower angles. Possible weak regions in the Tyrrhenian might be inherited pre-existing tectonic features that can be reactivated. Field work on Elba Island shows that extensional features related to the opening of the Northern Tyrrhenian Sea overprint former compressional features [*Keller and Coward*, 1996]. Thus, the initial angle of the major normal faults may have been controlled by the reactivation of relatively high-angle thrust faults.

[51] The higher heat flow in the northeastern Tyrrhenian is in agreement with a lithospheric thickness of just 30 km in the Tuscany region just north of our study area [*Contrucci et al.*, 2005]. The thermal state of this area suggests that the crust might have been thermally weakened, because the present heat flow in this area locally exceeds values of ~100 mW/m². *Allemand and Brun* [1991] showed from field data and experimental modeling, that if faults are generated at angles <50°, the brittle-ductile transition is located in the crust and a ductile lower crust therefore exists. Hence, it is possible that increased heat flow might have been present prior to active rifting, thereby explaining the initial fault angles of 45°–50°. Higher thermal gradients would influence the depth at which rocks behave brittly (<300°C–400°C) or ductily

(>400°C) [*Odedra et al.*, 2001]. This means that at a depth of 3–4 km underneath the seafloor, rocks start to behave ductily and thus deeper brittle faulting should be constrained to above these depths.

6.3.3. Detachments and Low-Angle Normal Faults

[52] Asymmetry of the tectonic structure of rift systems is often associated with the existence of large-scale long-lived detachment faults that cut the entire crust or perhaps even the whole lithosphere [e.g., *Bosworth*, 1985; *Wernicke*, 1985]. Most studies have interpreted rifted structures after break up, but in the northern Tyrrhenian Sea, our profile provides an image of the structure during the early period of asymmetric development. The existence of crustal-scale low-angle normal faults or long-lived detachments in the northern Tyrrhenian basin seems implausible for of two reasons. First, there is no evidence in the seismic images for shallow dipping intracrustal features giving rise to top of basement faults, similar to those observed in oceanic core complexes [e.g., *Ranero and Reston*, 1999]. In general, detachment faults are active in the brittle domain and thus, their presence in the northern Tyrrhenian segment should be relatively shallow and they should be easily detectable with seismic methods. Second, estimations of total fault displacement (β_f and β_{pb}) do not require additional slip on large-scale low-angle faults, since the estimated extension matches the amount of entire crustal thinning (β_v). Although a low-angle fault exists onshore Elba (Zuccale fault), its formation is assumed to be related to the presence of foliated mineral phases that makes the fault weak [*Collettini et al.*, 2009]. While such structures may exist, our data indicate that they do not play an important role accommodating space during the early rifting phase. At other regions in an early-rifting stage, it has been shown that low-angle faults are not necessary to explain extension, for example in the Gulf of Corinth [*Bell et al.*, 2008]. Seismic images from the Porcupine Basin and the Deep Galicia Margin reveal structures that have been interpreted as low-angle detachment faults that may have been active at high stretching factors (larger than ~3). However, those features have not been observed in the parts of the Porcupine Basins where the extension is considerably less [*Reston et al.*, 2004].

6.4. Implications for Early-Stage Continental Rifting

[53] Comparison of these results with previous studies of other young rift basins such as the Gulf of Corinth, the Suez Rift or Lake Baikal (Figure 12) reveals that the formation of half-graben structures by strain localization mechanisms on major normal faults is commonplace for the early phases of stretching. The rift initiation is not controlled by the formation of long-lived detachment faults and it can be considered to be the normal style of rifting for continental crust with small extension factors ($\beta < 1.3$). Crustal stretching and thinning is distributed homogeneously across the northern segment of the Tyrrhenian Sea and suggests that additional slip on shallow dipping detachments that link fault-bounded blocks such as offshore Iberia [*Ranero and Pérez-Gussinye*, 2010] or like those in the Porcupine Basin, develop only with larger stretching factors [*Reston et al.*, 2004].

[54] The pre-rift temperature-gradient controls the thickness of the brittle and ductile layers and might have controlled the initiation angle of faults in the Tyrrhenian basin at shallower dip angles than standard rheology predicts. In the lower part of the crust where the temperature exceeds 350°–400°, rocks undergo ductile deformation by an amount of stretching that is roughly similar to that obtained by shallower brittle faulting (Figure 12d).

7. Conclusions

[55] The study of the northern Tyrrhenian Basin, contributes to the basic understanding of the processes of early continental extension. We analyzed new WAS data as well as a prestack depth-migrated image of multichannel seismic data between Corsica and Italy. We found two domains, each with a distinct tectonic style and crustal thickness. The 6 km deep Corsica Basin in the west developed mainly during an older rift-phase in the Oligocene. The basin is filled with post-tectonic Early-Pliocene to Quaternary sedimentary deposits. Beneath, the Messinian to Langhian and older sediments together form a fan-shaped syn-tectonic sequence. Tomographic inversion shows that the crystalline crust has thinned to ~15 ± 1 km with velocities ranging from 6.0 km/s at the top to 6.7 km/s at the base of the crust. The depth-migrated image shows that the Corsica Basin is bounded by a ~10 km deep westward dipping sedimentary complex near the Pianosa Ridge.

[56] East of the Corsica Basin, a second domain exhibit rifted crust at the center of the northern Tyrrhenian segment and the Latium Margin. Two unconformities mark the active rift phase

confining syn-tectonic deposits of late Tortonian, Messinian and Early-Pliocene age. The area subsided and developed prominent tilted blocks and asymmetric half-graben structures by rotation on 10 major faults. We found that the crust has been stretched by a factor β_f of ~ 1.30 and that the majority of extension was localized by the displacements on surface-breaking major faults. Furthermore, we found that major faults dip $30°$–$40°$ to the east and rotated beds in the hanging wall dip $\sim 12°$ to the west. This suggests an initial fault angle of $\sim 45°$–$50°$. Tomographic inversion reveals a $\sim 17 \pm 1$ km thick crust and a subhorizontal Moho which is well constrained by PmP-reflections. Upper crustal velocities below the thin sedimentary cover represent typical values for continental crust (3.5–6.0 km/s). Velocities in the lower crust are slightly higher (6.6–6.8 km/s), presumably related to a higher proportion of mafic minerals. Assuming an initial crustal thickness of 24 km, as is currently observed under Corsica, the crustal thickness of the basin obtained by inversion of wide angle data indicates a crustal thinning of $\sim 30\%$. This result matches the horizontal stretching estimated from fault displacements. Thus, there is no extension discrepancy. Moreover, crustal-scale detachment faults should be imaged in the seismic data but are not. Assuming that the duration of the main rift activity lasted 3–4 Ma and taking into account the total horizontal displacement, the opening rate of this basin can be calculated to be between 7.8 and 10.3 mm/a.

[57] We propose that the young northern Tyrrhenian Basin evolved homogeneously by stretching and block rotation in the brittle upper crust and ductile deformation in the lower crust. Other young rift basins, like the Gulf of Corinth, the Suez Rift, or Lake Baikal resemble the northern Tyrrhenian Basin to a large extent. This may suggest that half-graben formation and distributed, homogeneous crustal thinning is a common feature during rift initiation. Furthermore, seismic images reveal no evidence for low-angle detachment faulting in the main part of the basin. Again, this is similar to other young rift basins elsewhere and may imply that detachment faults do not develop until higher stretching factors are reached.

Acknowledgments

References

Abers, G. A. (2009), Slip on shallow-dipping normal faults, *Geology*, *37*(8), 767–768, doi:10.1130/focus082009.1.

Allemand, P., and J.-P. Brun (1991), Width of continental rifts and rheological layering of the lithosphere, *Tectonophysics*, *188*, 63–69.

Bell, R. E., L. C. McNeill, J. M. Bull, and T. J. Henstock (2008), Evolution of the offshore western gulf of corinth, *Geol. Soc. Am. Bull.*, *120*(1-2), 156–178.

Bosworth, W. (1985), Geometry of propagating continental rifts, *Nature*, *316*(6029), 625–627, doi:10.1038/316625a0.

Buck, R. W. (1993), Effect of lithospheric thickness on the formation of high- and low-angle normal faults, *Geology*, *21*, 933–936, doi:10.1130/0091–7613(1993)021<0933:EOLTOT>2.3.CO;2.

Cherchi, A., and L. Montadert (1982), Oligo-Miocene rift of Sardinia and the early history of the Western Mediterranean Basin, *Nature*, *298*, 736–739, doi:10.1038/298736a0.

Christensen, N. I., and W. D. Mooney (1995), Seismic velocity structure and composition of the continental crust: A global view, *J. Geophys. Res.*, *100*(B6), 9761–9788, doi:10.1029/95JB00259.

Collettini, C., A. Niemeijer, C. Viti, and C. Marone (2009), Fault zone fabric and fault weakness, *Nature*, *462*(7275), 907–910.

Contrucci, I., A. Mauffret, C. Brunet, A. Nercessian, N. Béthoux, and J. Ferrandini (2005), Deep structure of the North Tyrrhenian Sea from multi-channel seismic profiles and on land wide angle reflection/refraction seismic recording (LISA cruise): Geodynamical implications, *Tectonophysics*, *406*(3–4), 141–163, doi:10.1016/j.tecto.2005.05.015.

Della Vedova, B., Pellis, G., J. P. Foucher, J.-P. Rehault (1984), Geothermal structure of the Tyrrhenian Sea, *Mar. Geol.*, *55*, 271–289.

Derer, C. E., M. E. Schumacher, and A. Schaefer (2005), The northern upper Rhine graben: Basin geometry and early syn-rift tectono-sedimentary evolution, *Int. J. Earth Sci.*, *94*, 640–656, doi:10.1007/s00531-005-0515-y.

Faccenna, C., T. W. Becker, F. P. Lucente, L. Jolivet, and F. Rossetti (2001), History of subduction and back-arc extension in the Central Mediterranean, *Geophys. J. Int.*, *145*, 809–820, doi:10.1046/j.0956-540x.2001.01435.x.

Gawthorpe, R. L., C. A.-L. Jackson, M. J. Young, I. R. Sharp, A. R. Moustafa, and C. W. Leppard (2003), Normal fault growth, displacement localization and the evolution of normal fault populations: The hammam faraun fault block, Suez rift, Egypt, *J. Struct. Geol.*, *25*(6), 883–895.

Hutchinson, D. R., A. J. Golmshtok, L. P. Zonenshain, T. C. Moore, C. A. Scholz, and K. D. Klitgord (1992),

Depositional and tectonic framework of the rift basins of Lake Baikal from multichannel seismic data, *Geology*, *20*, 589–592, doi:10.1130/0091–7613(1992)020<0589:DATFOT>2.3.CO;2.

Jackson, J. A. (1987), Active normal faulting and crustal extension, *Geol. Soc., London Spec. Publ.*, *28*(1), 3–17.

Jolivet, L., D. Frizon de Lamotte, A. Mascle, and M. Seranne (1999), The Mediterranean Basins: Tertiary extension within the Alpine Orogen—An introduction, *Geol. Soc. Spec. Publ.*, *156*, 1–14, doi:10.1144/GSL.SP.1999. 156.01.02.

Kastens, K. A., et al. (1988), ODP Leg 107 in the Tyrrhenian Sea: Insights into passive margin and back-arc basin evolution, *Geol. Soc. Am. Bull.*, *100*, 1140–1156, doi:10.1130/0016–7606(1988)100<1140:OLITTS>2.3.CO;2.

Keller, J. V. A., and M. P. Coward (1996), The structure and evolution of the Northern Tyrrhenian Sea, *Geol. Mag.*, *133*, 1–16, doi:10.1017/S0016756800007214.

Korenaga, J., W. S. Holbrook, G. M. Kent, P. B. Kelemen, R. S. Detrick, H.-C. Larsen, J. R. Hopper, and T. Dahl-Jensen (2000), Crustal structure of the southeast Greenland margin from joint refraction and reflection seismic tomography, *J. Geophys. Res.*, *105*(B9), 21,591–21,614, doi:10.1029/2000JB900188.

Lister, G. S., M. A. Etheridge, and P. A. Symonds (1991), Detachment models for the formation of passive continental margins, *Tectonics*, *10*(5), 1038–1064.

Malinverno, A., and W. B. F. Ryan (1986), Extension in the Tyrrhenian Sea and shortening in the Apennines as result of arc migration driven by sinking of the lithosphere, *Tectonics*, *5*(2), 227–245, doi:10.1029/TC005i002p00227.

Marett, R., and R. W. Allmendinger (1992), Amount of extenison on "small" faults: An example from the Viking graben, *Geology*, *20*, 47–50, doi:10.1130/0091.

Mauffret, A., I. Contrucci, and C. Brunet (1999), Structural evolution of the Northern Tyrrhenian Sea from new seismic data, *Mar. Pet. Geol.*, *16*(5), 381–407, doi:10.1016/S0264–8172(99)00004–5.

McKenzie, D. (1978), Some remarks on the development of sedimentary basins, *Earth Planet. Sci. Lett.*, *40*, 25–32.

Medimap (2008), CIESM/Ifremer Medimap Group, Loubrieu B., Mascle J. et al., Morpho-bathymetry of the Mediterranean Sea.

Mele, G., and E. Sandvol, (2003), Deep crustal roots beneath the northern Apennines inferred from teleseismic receiver functions, *Earth Planet. Sci. Lett.*, *211*(1–2), 69–78, doi:10.1016/S0012–821X(03)00185-7.

Odedra, A., M. Ohnaka, H. Mochizuki, and P. Sammonds (2001), Temperature and pore pressure effects on the shear of strength of granite in the Brittle-Plastic Transition Regime, *Geophys. Res. Lett.*, *28*(15), 3011–3014, doi:10.1029/2001GL013321.

Pérez-Gussinyé, M., C. R. Ranero, T. J. Reston, and D. Sawyer (2003), Structure and mechanisms of extension at the Galicia Interior Basin, West of Iberia, *J. Geophys. Res.*, *108*(B5), 2245, doi:10.1029/2001JB000901.

Ponziani, F., R. De Franco, G. Minelli, G. Biella, C. Federico, and G. Pialli (1995), Crustal shortening and duplication of the Moho in the Northern Apennines: A view from seismic refraction data, *Tectonophysics*, *252*(1–4), 391–418, doi:10.1016/0040–1951(95)00093-3.

Ranero, C. R., and T. J. Reston (1999), Detachment faulting at Inside Corners, *Geology*, *27*, 983–986.

Ranero, C. R., and M. Pérez-Gussinye (2010), Sequential faulting explains the asymmetry and extension discrepancy of conjugate margins, *Nature*, *468*, 294–300, doi:10.1038/nature09520.

Reston, T. (2007), Extension discrepany at North Atlantic non-volcanic rifted margins: Depth-dependent stretching or unrecognized faulting?, *Geology*, *35*, 367–370, doi:10.1130/G23213A.1.

Reston, T. J., V. Gaw, D. Klaeschen, A. Stubenrauch, and I. Walker (2004), Extreme crustal thinning in the south Porcupine Basin and the nature of the Porcupine Median High: Implications for the formation of non-volcanic rifted margins, *J. Geol. Soc.*, *161*, 783–798, doi:10.1144/0016–764903-036.

Rosenbaum, G., G. S. Lister, and C. Duboz (2002), Reconstruction of the tectonic evolution of the western Mediterranean since the Oligocene, *J. Virtual Explor.*, *8*, 107–130, doi:10.3809/jvirtex.2002.00053.

Sartori, R. (1990), The main results of ODP Leg 107 in the frame of neogene to recent geology of perityrrhenian areas, *Proc. Ocean Drill. Program Sci. Results*, *107*, 715–730.

Sartori, R., L. Torelli, N. Zitellini, G. Carrara, M. Matteo, and P. Mussoni (2004), Crustal features along a W–E Tyrrhenian transect from Sardinia to Campania margins (Central Mediterranean), *Tectonophysics*, *383*(3–4), 171–192, doi:10.1016/j.tecto.2004.02.008.

Schellart, W. P. (2010) Mount-Etna-Iblean volcanism caused by rollback-induced upper mantle upwelling around the Ionian slab edge: An alternative to the plume model, *Geology*, *38*(8), 691–694.

Shillington, D. J., W. S. Holbrook, H. J. A. Van Avendonk, B. E. Tucholke, J. R. Hopper, K. E. Louden, H. C. Larsen, and G. T. Nunes (2006), Evidence for asymmetric nonvolcanic rifting and slow incipient oceanic accretion from seismic reflection data on the Newfoundland margin, *J. Geophys. Res.*, *111*, B09402, doi:10.1029/2005JB003981.

Trincardi, F., and N. Zitellini (1987), The rifting of the Tyrrhenian Basin, *Geo Mar. Lett.*, *7*, 1–6, doi:10.1007/BF02310459.

Wang, C. Y., W. T. Hwang, and Y. Shi (1989), Thermal evolution of a Rift Basin: The Tyrrhenian Sea, *J. Geophys. Res.*, *94*(B4), 3991–4006.

Walsh, J., J. Watterson, and G. Yielding (1991), The importance of small-scale faulting in regional extensions, *Nature*, *351*, 391–393, doi:10.1038/351391a0.

Wernicke, B. (1985), Uniform-sense normal simple shear of the continental lithosphere, *Can. J. Earth Sci.*, *22*, 108–125.

Wessel, P., and W. H. F. Smith (1998), New, improved version of the Generic Mapping Tools Released, *EOS Trans. AGU*, *79*, 579.

Wernicke, B., and C. B. Burchfiel (1982), Modes of extensional tectonics, *J. Struct. Geol.*, *4*(2), 105–115, doi:10.1016/ 0191–8141(82)90021-9.

White, N. (1990), Does the uniform stretching model work in the North Sea?, in *Tectonic Evolution of the North Sea Rifts*, edited by D. J. Blundell and A. D. Gibbs, *Intl. Lithosphere Progr. Pub. 181*, 217–239.

Zelt, C. A., and R. B. Smith (1992), Seismic traveltime inversion for 2-D crustal velocity structure, *Geophys. J. Int.*, *108*, 16–34, doi:10.1111/j.1365-246X.1992.tb00836.x.

Zitellini, N., F. Trincardi, M. Marani, and A. Fabbri (1986), Neogene tectonics of the northern Tyrrhenian Sea, *Giornale Geol.*, *48*, 25–40.